Available online at www.sciencedirect.com

ScienceDirect

Physics Procedia 56 (2014) 1268 – 1276

Physics Procedia

8th International Conference on Photonic Technologies LANE 2014

Experimental and numerical analysis of gas dynamics in the keyhole during laser metal welding

Felix Tenner[a,b,*], Christian Brock[a,b], Franz-Josef Gürtler[a,b], Florian Klämpfl[a], Michael Schmidt[a,b,c]

[a] *Institute of Photonic Technologies (LPT), Friedrich-Alexander-Universität Erlangen-Nürnberg, Konrad-Zuse-Str. 3/5, 90152 Erlangen, Germany*
[b] *Erlangen Graduate School in Advanced Optical Technologies (SAOT), Friedrich-Alexander-Universität Erlangen-Nürnberg, Paul-Gordan Str. 6, 90152 Erlangen, Germany*
[c] *Bayerisches Laserzentrum GmbH (blz), Konrad-Zuse-Str. 2-6, 90152 Erlangen, Germany*

Abstract

The keyhole is the crucial factor for an appropriate weld seam in laser metal welding. The stability of the keyhole is governed by multiple hydrodynamic effects such as melt flow, evaporation on the keyhole front, gas dynamics inside the evolving vapor plume and the resulting pressures from all these phenomena. Due to their elusive nature the measurement of pressures inside the keyhole is still an unresolved task. Here we show a quantification of the density of the metal vapor and the pressure inside the keyhole through measuring the keyhole opening geometry, the evaporation rate and the flow velocity inside the vapor plume. Furthermore, a comparison to a simulation model is shown. Our results are in accordance with theoretical approaches. In the future this results can support an increase of process understanding which eventually leads to a better control of the process in industry.

Peer-review under responsibility of the Bayerisches Laserzentrum GmbH

Keywords: laser material processing; laser welding; high-speed camera; numerical simulation; vapor pressure

1. Introduction

Even though widely applied in industry, laser welding still offers many challenges for researchers trying to understand the involved physics. Especially when the discussion turns to the formation of weld defects like pores, spatter or weld seam irregularities, each team of researchers seems to have their own explanation and model. On the bottom line, however, it is agreed that the keyhole, or more precisely the keyhole geometry and its stability, are responsible for the quality of the resulting weld seam Dowden (2009). Therefore, we try to predict and quantify the factors which influence the keyhole geometry. Finally, this knowledge could be used to control the process by monitoring the intrinsic influencing factors.

* Corresponding author. Tel.: +49-9131-85-23236 ; fax: +49-9131-85-23234 .
E-mail address: felix.tenner@lpt.uni-erlangen.de

Peer-review under responsibility of the Bayerisches Laserzentrum GmbH
doi:10.1016/j.phpro.2014.08.050

2. State of the art

In deep penetration laser welding, the shape and stability of the keyhole emerge from a balance of counteracting forces: On one side evaporation induced recoil pressure drives the molten metal away from the center of the keyhole, whereas on the other side surface tension and hydrodynamic pressure force the liquid inwards and tend to close the keyhole as shown from Hirano et al. (2011).

Since the generation of the first keyhole in the early seventies published from Locke et al. (1972), several theoretical models have been proposed describing the optical, thermal and fluid dynamic mechanisms involved in the process (for example by Knight (1972); Semak and Matsunawa (1997); Seidgazov (2009)). Subsequently, experiments have been performed trying to verify the predictions made by these models. Up to day, direct measurements of the keyhole shape using x-ray systems (Katayama et al. (2010); Abt et al. (2011)), high speed recordings of the fluid dynamics at the keyhole front (Eriksson et al. (2013) and of the melt flow in the melt pool behind the keyhole (Fabbro et al. (2007)) have been performed. Furthermore, several studies on the vapor plume, formed by hot metal vapor ejected from the keyhole, have been carried out in order to find correlations between vapor plume and keyhole properties (published from Fabbro (2010); Sibillano et al. (2012); Tenner et al. (2013); Brock et al. (2013)).

As we will discuss in this paper, the velocity of the metal vapor streaming out of the keyhole is linked to the pressure inside the keyhole, and therefore provides a means to study the welding process. Theoretical studies report vapor velocities of 11 $\mathrm{m\,s^{-1}}$ (Courtois et al. (2013)), 20 $\mathrm{m\,s^{-1}}$ (Zhang et al. (2011)) and 40 $\mathrm{m\,s^{-1}}$ (Amara et al. (2006)). It seems that only one experimental approach by Sokolowinski (1991) was published so far: Using a streak camera a vapor velocity of 10 $\mathrm{m\,s^{-1}}$ was measured during keyhole welding with a CO_2 laser.

In this paper, we measured the velocity of the metal vapor inside the plume during Yb:YAG welding of steel sheets for several feed rate and laser power settings. Additionally, we recorded the properties of the keyhole opening at the workpiece surface and determined evaporation rates using a balance, which enables us to calculate the density of the metal vapor and to estimate the keyhole pressure.

3. Experimental

To study the dynamic behavior of the keyhole and the plasma plume simultaneously we used two high-speed cameras (VisionResearch Phantom v1210) working with a frame rate of 100 kHz using an image size of 256 x 256 pixel. We used a laser system (Cavitar Cavilux HF, 807 nm, 500 W peak power) to illuminate the keyhole region. Using a band-pass filter in front of the camera that imaged the keyhole region, we ensured that only the wavelength of the illumination laser reached the imaging chip of that camera. All other disturbing light (e.g. the brightness of the plasma plume and the reflections of the processing laser from the melt pool) were blocked or reduced.

For material processing we used a TruDisk 4002 Yb:YAG laser (wavelength 1030 nm, maximum output power 4 kW) coupled to focusing optics (BEO D70, focal length 200 mm, spot size 600 μm, beam profile *top hat*). We applied this setup to weld two stainless steel plates (X6CrNiTi18-10) of 1 mm thickness in an overlap configuration. Furthermore, we used a system of linear axis (Aerotech PRO280LM) for moving the metal sheets with constant feed rates from 2 to 7 $\mathrm{m\,min^{-1}}$. For the isochronous observation of the keyhole and the plasma plume camera 1 was lined up at a 55 $^\circ$ angle to the metal sheets and a objective with a magnification of 1.5 was installed to have a detailed view of the keyhole. The camera 2 was positioned perpendicular to the feeding direction at a 10 $^\circ$ angle to look at the plasma plume from its point of formation (the keyhole) to the top (see Fig. 1).

3.1. Image evaluation

To analyze the dynamic behavior the scenery was imaged at high speed, so the uncertainty due to the high process dynamics was minimized (as compared with previous studies). Due to the high camera frame rate an algorithm is required to evaluate the 100,000 images per second in a fast and reliable way.

For evaluating the keyhole area we used an algorithm consisting of threshold operations and morphological filters (Serra and Vincent (1992)) with Matlab. To quantify the flow velocity of the vapor plume an optical flow algorithm from Farnebäck (2003) was applied. This algorithm tracks the changes in the position of neighboring bright pixels from consecutive images. This information can be expressed in vectors. With the use of a calibration pattern

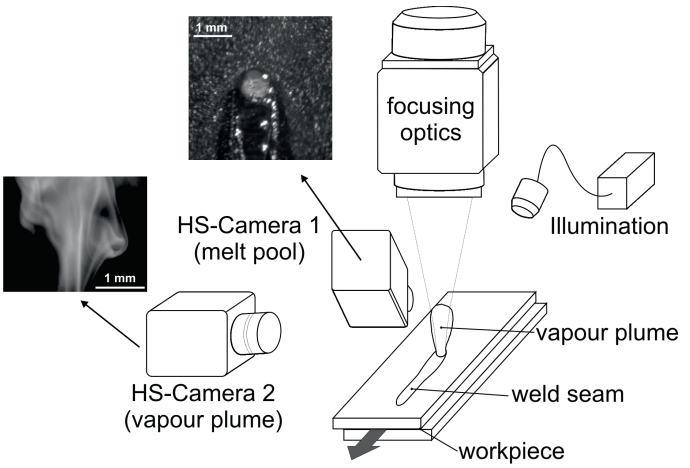

Fig. 1. Imaging setups for isochronous keyhole and plasma plume observation.

and the knowledge of the frame rate it is possible to convert the flow velocity from *pixel per frame* to *meters per second*.

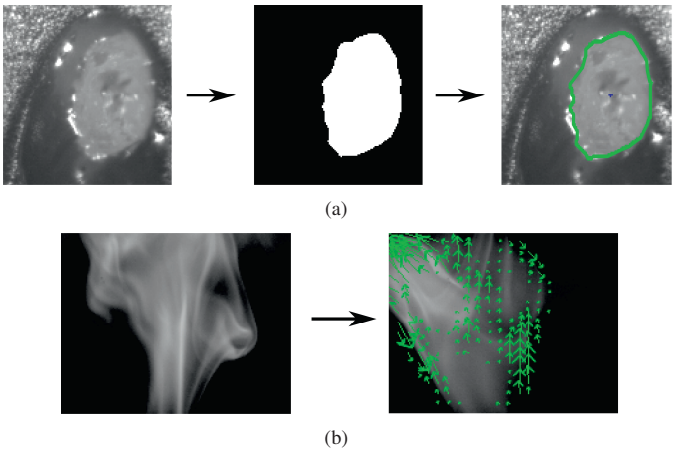

(a)

(b)

Fig. 2. Image evaluation of the keyhole opening area (a) and the flow of the vapor plume (b).

Fig. 2 shows the outcome of both evaluation algorithms. Fig. 2(a) illustrates the detected contour of the keyhole opening area (shown with a green line). Fig. 2(b) shows the vectors which visualize the movement of the plasma plume.

4. Results and discussion

4.1. Analysis of the metal vapor properties

In a first set of welding experiments, we performed welds with feed rates of 2 and 4 m min^{-1} and different laser power settings and determined the area of the keyhole opening A_k and the vapor velocity v_v as described in section 3. We measured v_v within a range of 1 mm above the keyhole opening where the vapor has not expanded significantly yet and shows nearly no turbulent flow. Furthermore, we determined the mean evaporation rate $\dot{m}$ by weighing the workpiece before and after the weld. We calculated the mean value of v_v and A_k, repeated the experiment twice with

the same laser power and feed rate setting and then calculated the mean of the three experiments. Fig. 3 shows the mean keyhole opening area (a), the mean vapor velocity (b) and the mean evaporation rate (c) obtained by weighing, for feed rates of 2 m min^{-1} and 4 m min^{-1} and different laser power settings. A_k, v_v and $\dot{m}$ increase when we increase the laser power.

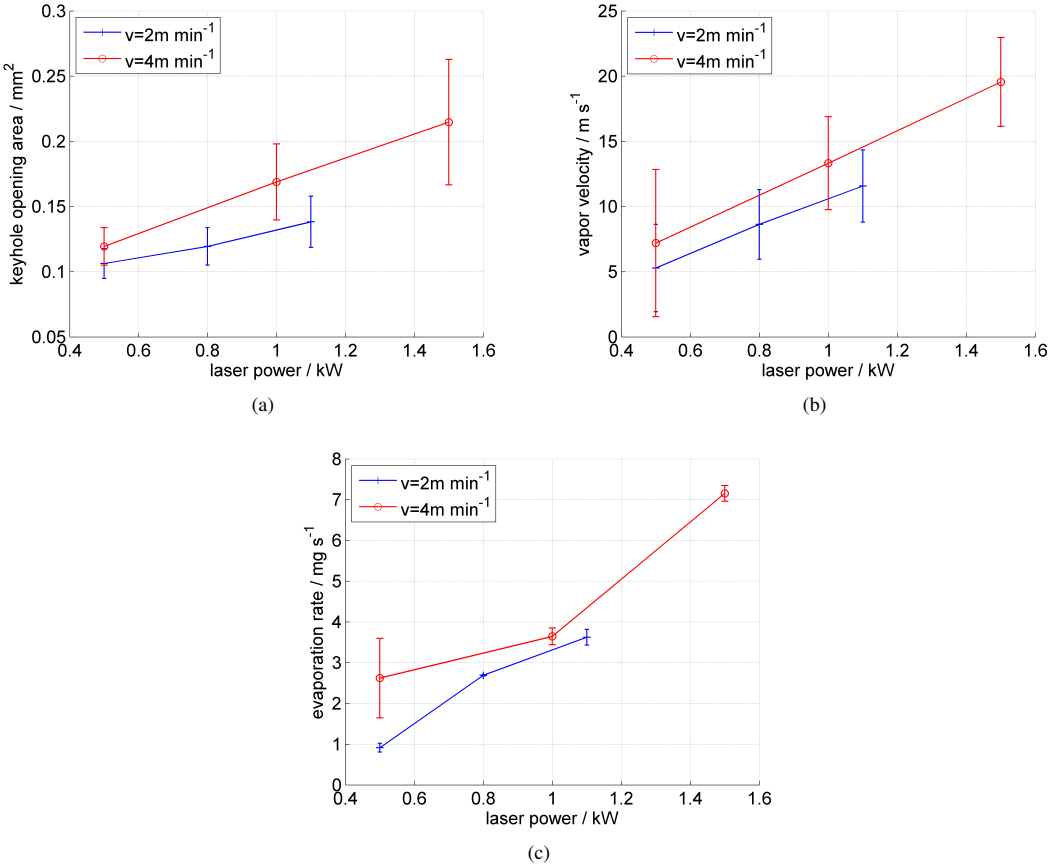

Fig. 3. Dependence of the keyhole opening area (a), the vapor velocity (b) and the evaporation rate (c) on the laser power and feed rates (2 m min^{-1} and 4 m min^{-1}). Each data point represents the mean of three experiments with the same welding parameters, the errorbars indicate the corresponding standard deviation.

It is important to note that the determination of the evaporation rate is possible only in a certain range of laser power settings: The high speed image sequences show that if we increase the laser power above 1.1 kW (1.5 kW) for a feed rate of 2 m min^{-1} (4 m min^{-1}) spatter occurs, whereas no spatter formed for lower laser power settings. Since the formation of spatter leads to a considerable loss of weight of the workpiece, we cannot use welds where we observed spatter for the determination of the evaporation rate.

The high speed sequences of the keyhole opening and cross-sections show that for a laser power of 0.5 kW the melt pool only contains a slight depression, whereas for higher laser power settings this depression grows and a keyhole forms.

In the following section we discuss the reason for the increasing trends of the vapor velocity, the area of the keyhole opening and of the evaporation rate. When we increase the laser power, we introduce more energy into the workpiece. That means that more heat is available for evaporation and consequently the evaporation rate increases. Furthermore, the keyhole depth increases, resulting in better absorption by multiple reflections and thus to a further increase of the evaporation rate. The increase of evaporation causes an increase of recoil pressure onto the keyhole surface. Hence,

a widening of the keyhole seems reasonable. However, the increasing evaporation is not completely compensated by keyhole expansion: Since we observe that the vapor velocity increases with the laser power, we conclude that a part of the increasing evaporation causes an acceleration of the vapor particles.

Considering the stream of vapor particles through the keyhole opening with an area A_k, conservation of mass (Akshoy et al. (2005)) leads to

$$\dot{m} = \rho_v A_k v_v, \tag{1}$$

i.e. the mass flow rate $\dot{m}$ (which in our case is given by the evaporation rate) through the keyhole opening increases with the density of the metal vapor ρ, the keyhole opening area A_k and with the vapor velocity v_v. Since we measured $\dot{m}$, A_k and v_v, we can calculate ρ using equation 1. Fig. 4 shows the vapor density calculated using the data from Fig. 3. Since no clear trend is distinguishable, we will assume that the vapor density does not significantly vary during our welding experiments and use the mean value of all data points shown in figure 4 in the following section, which is $\rho_v = (2.8 \pm 2.4)\,\mathrm{kg\,m^{-3}}$. This is only a rough estimation. Nevertheless, it is in accordance with other publications as shown in the next paragraph.

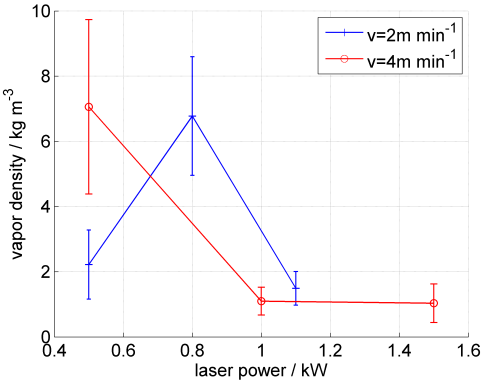

Fig. 4. vapor density calculated using Eq. 1 and the data from Fig. 3; n=3.

Extinction measurements of the vapor plume at fiber laser welding by Shcheglov et al. (2011) yielded a particle density of $10 \times 10^{10}\,\mathrm{cm^{-3}}$ and a mean particle diameter of 77 nm, corresponding to a vapor density of $0.15\,\mathrm{kg\,m^{-3}}$. The extinction measurement was performed via the measurement of the attenuation of a He-Ne-Laser directed through the vapor plume at a height of 10 mm above the keyhole opening. Here the vapor most probably has expanded, which explains the difference to our result. Comparing to theoretical studies, we see that the value of ρ_v obtained in this work is in rough agreement with the results of Mundra and Debroy (1993), DebRoy et al. (1991) and Courtois et al. (2013), where vapor densities of $0.7\,\mathrm{kg\,m^{-3}}$, $1\,\mathrm{kg\,m^{-3}}$ and $10\,\mathrm{kg\,m^{-3}}$ were calculated.

4.2. Estimation of the keyhole pressure

In the experiments discussed so far, we used low laser power settings in order to avoid spatter formation. In a second set of experiments we measured the vapor velocity for higher laser power settings as well, where spatter formed (Fig. 5(a)). We applied feed rates of $2\,\mathrm{m\,min^{-1}}$, $4\,\mathrm{m\,min^{-1}}$ and $7\,\mathrm{m\,min^{-1}}$ and increased the laser power stepwise until full penetration was reached. Using the metal vapor density determined in section 4.1, we can now calculate the dynamic pressure $p_{dyn} = \frac{1}{2}\rho_v v_v^2$ of the metal vapor. p_{dyn} represents the pressure of the metal vapor remaining after having forced aside the surrounding air, which exerts a pressure $p_0 = 101\,\mathrm{kPa}$ (atmospheric pressure) onto the keyhole. Therefore, we can calculate the pressure p_k inside the keyhole (which, as discussed in section 1, predominantly determines the state of the keyhole) by simply adding p_0 to the measured dynamic pressure:

$$p_k = p_0 + p_{dyn} \tag{2}$$

By doing so, however, we neglect recondensation of vapor particles inside the keyhole. Recondensation weakens the vapor jet, so that Eq. 2 underestimates p_k by a factor given by the recombination rate β_R. In a publication

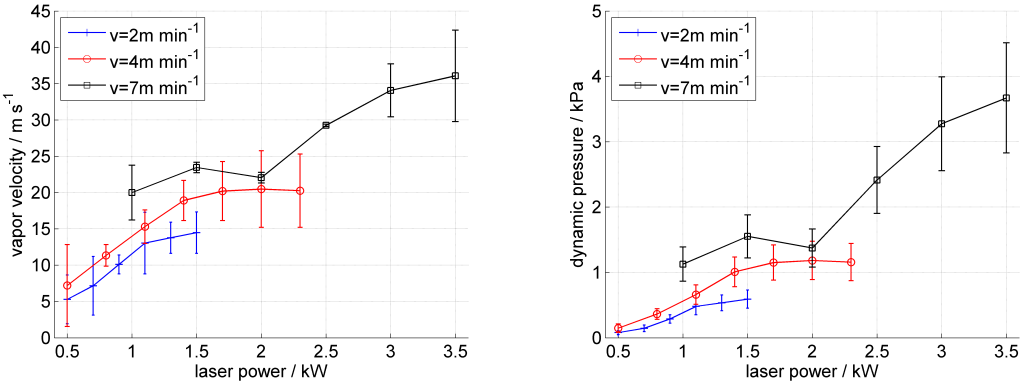

(a) (b)

Fig. 5. (a) Velocity of the metal vapor for the extended range of welding parameters. (b) Dynamic pressure $p_{dyn} = \frac{1}{2}\rho_v v_v^2$ of the metal vapor calculated using the vapor velocities shown in (a); n=3.

from Miyamoto and Maruo (1996) it is concluded that "most metal vapor produced within the keyhole was deposited again on the wall surface", and according to Hirano et al. (2011) recombination rates of up to $\beta_R = 0.9$ are possible in case of keyhole welding. That means that evaporation in the keyhole may actually be up to 10 times stronger than indicated by the evaporation rate we measured at the keyhole opening. Based on the dynamic pressure of the vapor plume shown in Fig. 5(b) which is in the order of 1 kPa, we estimate the mean keyhole pressure to $p_k \simeq p_0 + 10 p_{dyn}$ = 111 kPa. In our experiments the keyhole pressure increases up to 140 kPa and may increase even further with increasing laser power and velocity. However, there is a slight saturation visible for every velocity in Fig. 5(b). This saturation could originate from the increase of the keyhole depth and therefore an increase in recondensation inside the keyhole which in turn affects the recombination rate β_R.

5. Comparison to simulation model

5.1. Physical model

The scientific findings of the experiments should be compared with our simulation model for laser material processing (Otto and Schmidt (2010); Koch et al. (2011)). The model uses the open source computational fluid dynamics (CFD) software package OpenFOAM© (Open Field Operation and Manipulation). Many physical effects are considered in this model. The flow and the energy flux of the vapor, fluid and solid phases are calculated by partial differential equations. The flow characteristic is specified as an incompressible fluid by the Navier-Stokes equation (Versteeg and Malalasekera (2007)). The gas-liquid transition zones are described as free surfaces under the use of the volume of fluid (VOF) approach (Ferziger and Perić (2008)). Furthermore, the heat conduction and the latent heat of melting and evaporation are included (Ki et al. (2001)). The spatial and temporal discretization of the model is depending on the process dynamics. The size of time steps is controlled by the help of the Courant number (Courant et al. (1928)). The cubic mesh is automatically adapted by refinement and unrefinement for accurate calculations and manageable calculation times.

5.2. Results of the simulation model and comparison to experiments

The welding parameters for the simulations are the same as in the experiments in section 4.1. Only the examined area was reduced to a length of 7 mm and a width of 2 mm. Around the metal sheets an atmosphere exists (2 mm below and 10 mm above the sheets). The laser beam center was moving in a distance of 1 mm to the boundaries. With this model we analyzed the feed rates of 2 m min^{-1} and 4 m min^{-1} at different laser power levels.

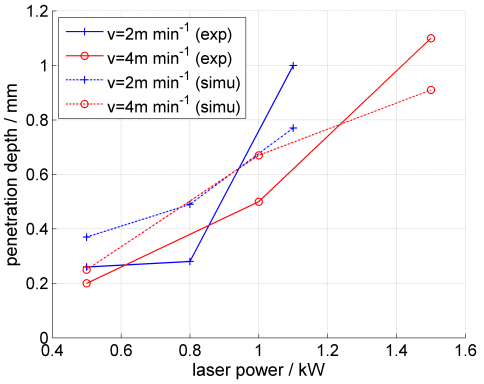

Fig. 6. Penetration depths of the simulations depending on the laser power and feed rates (2 m min^{-1} and 4 m min^{-1}) compared to the experiments.

A simple verification of the simulations is achieved by the examination of the penetration depth in the welded samples. The results of the simulation are shown in Fig. 6. For a low laser power of 500 W the simulation model does result in a heat conduction welding process. Therefore, just the welds with higher laser power were used for comparing the resulting gas velocity and dynamic pressure. For increasing laser power the penetration depth in the simulation model shows the same trend as in the experiments and the transition to deep penetration welding can be well modeled.

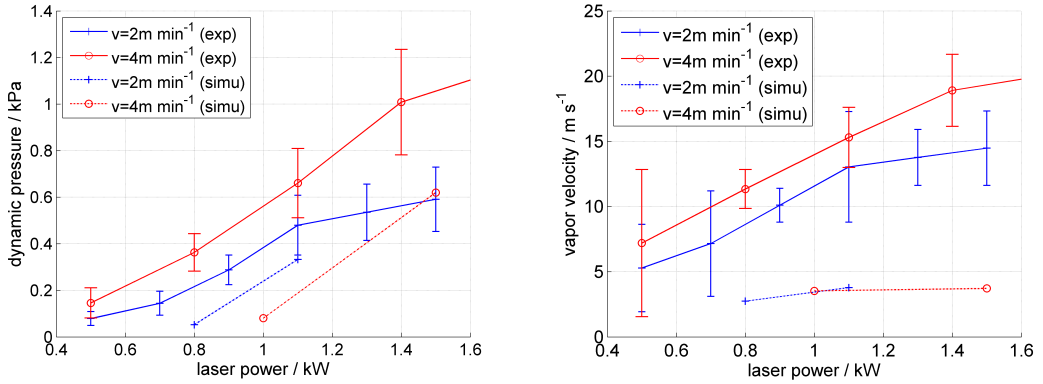

Fig. 7. Comparison of experiment and simulation: Dynamic pressure (a) and gas velocity (b) depending on the laser power and feed rates (2 m min^{-1} and 4 m min^{-1}); measured in the simulation 0.5 mm above the metal sheet in the laser beam center.

The velocity of the gas phase was measured 0.5 mm above the sheets in the laser beam center to have a comparable situation to the experimental results and to be more independent from the boundary conditions of our model. Furthermore, the dynamic pressure was measured to be compared to the pressure we calculated in the experiments. This comparison shows how good our assumptions in section 4.2 are.

The values we show are single point measurements under the conditions of spatial discretization. The results of the dynamic pressure are shown in Fig. (a). Due to the fact that a deep penetration welding process is just established for high laser power in the simulation it is obvious that a considerable dynamic pressure can just be modeled for high laser power. For medium laser power the dynamic pressure is very weak compared to our experimental measurements. Nevertheless, the trend for the dynamic pressure is the same as in our experiment and the initiation of deep penetration welding is well simulated.

Due to the fact that the dynamic pressure for low laser power is nearly zero in our modeled simulation we keep our focus on the vapor velocities for medium and high laser powers shown in Fig. 7(b). They show the same trend as the dynamic pressure. Nevertheless, compared to the experiments we can see a weaker trend of the vapor velocity. This may arise from the fact that the focus of our simulation model was mostly on modeling the pressure. An adjustment between the vapor velocities of our model and experiments was not done before this publication. Keeping this in mind and the fact that a modeling of the gas and fluid dynamics inside the keyhole is still a task of current research the trend of the vapor velocity and dynamic pressure inside the keyhole is well modeled.
The fact that the trend for the vapor velocity and the dynamic pressure is nearly equal in the simulation lead us to two conclusions:

1. The coincidences between the vapor velocity and the resulting dynamic pressure are well modeled in the simulation.
2. Our experimental approach to calculate the dynamic pressure from the keyhole opening area, the evaporation rate and the vapor velocity is in good agreement with the simulated trend.

In general the findings of simulations and experiments are comparable. The calculation of the dynamic pressure in the experiment in section 4.2 is meaningful. The simplifications are valid and the input parameters are wisely specified.

6. Conclusion and outlook

We showed an experimental approach for measuring the density of the metal vapor and the pressure inside the keyhole. Therefore, we measured the keyhole opening area and the flow velocity inside the vapor plume with high-speed imaging and the evaporation rate by weighing. With this experimental approach we ensured theoretical calculations and quantified the dependency of the measured values on the laser power and the feed rate. Based on a vapor velocity measurement fluctuations of the keyhole pressure could be quantified. Despite the fact that our calculations had some simplifications we agreed with the former theoretical work of other groups. Furthermore, simulations were computed and showed a good agreement in a qualitatively way.

In future work we would like to enhance the set of process parameters and try to verify our assumptions. Moreover, our simulation model will be improved with a more realistic modeling of the evaporation process and the gas dynamics. This may be solved by an increasing consideration of convection by a changed description of the vapor dynamics. Further improvement can be reached by temperature-dependent material parameters. Here we are also dependent on other fields of research to have more precise and reliable measurements of industry related materials like zinc-coated steel or high-alloyed steels. Finally, we plan to keep our focus more on industry related joining problems like the welding of zinc-coated steel sheets to prepare a basis for a process control which does not only monitor the impact of an unwelcome process dynamic, but the cause.

Acknowledgements

The authors gratefully acknowledge funding of the German Federal Ministry of Education and Research by the funding program Photonics Research Germany (contract number 13N12134) and funding of the Erlangen Graduate School in Advanced Optical Technologies (SAOT) by the German Research Foundation (DFG) in the framework of the German excellence initiative.

References

Abt, F., Boley, M., Weber, R., Graf, T., Popko, G., Nau, S., 2011. Novel x-ray system for in-situ diagnostics of laser based processes - first experimental results, in: Schmidt, M., Zaeh, M., Graf, T., Ostendorf, A. (Eds.), Physics Procedia, Volume 12, Part A, Elsevier. pp. 761–770.

Akshoy, R., Sanchayan, M., Pijush, R., 2005. Mechanical Sciences. Prentice Hall of India, New Delhi.

Amara, E., Fabbro, R., Hamadi, F., 2006. Modeling of the melted bath movement induced by the vapor flow in deep penetration laser welding. J. Laser Appl. 18(1), 2–11.

Brock, C., Tenner, F., Klämpfl, F., Hohenstein, R., Schmidt, M., 2013. Detection of weld defects by high speed imaging of the vapor plume, in: Emmelmann, C., Zaeh, M., Graf, T., Schmidt, M. (Eds.), Physics Proceedia, Vol 41: Lasers in Manufacturing (LiM 2013), Elsevier, Amsterdam. pp. 532–536.

Courant, R., Friedrichs, K., Lewy, H., 1928. Über die partiellen Differenzengleichungen der mathematischen Physik. Mathematische Annalen 100, 32–74.

Courtois, M., Carin, M., Le Masson, P., Gaied, S., 2013. A two-dimensional axially-symmetric model of keyhole and melt pool dynamics during spot laser welding. Revue de Mtallurgie 110, 165173.

DebRoy, T., Basu, S., Mundra, K., 1991. Probing laser induced metal vaporization by gas dynamics and liquid pool transport phenomena. J. Appl. Phys. 70(3), 1313–1319.

Dowden, J., 2009. The Theory of Laser Materials Processing. Springer, Dordrecht, The Netherlands.

Eriksson, I., Powell, J., Kaplan, A., 2013. Melt behavior on the keyhole front during high speed laser welding. Optics and Lasers in Engineering 51, 735740.

Fabbro, R., 2010. Melt pool and keyhole behaviour analysis for deep penetration laser welding. J. Phys. D: Appl. Phys. 43, 445501.

Fabbro, R., Slimani, S., Coste, F., Briand, F., 2007. Experimental study of the humping process during ndyag cw laser welding, in: Vollertsen, F., Emmelmann, C., Schmidt, M., Otto, A. (Eds.), Proceedings of the Fourth International WLT-Conference on Lasers in Manufacturing, WLT. pp. 277–282.

Farnebäck, G., 2003. Two-frame motion estimation based on polynomial expansion, in: Bigün, J., Gustavsson, T. (Eds.), Proceedings of the 13th Scandinavian Conference on Image Analysis, Halmstad, Sweden. Springer, Gothenburg and Sweden. pp. 363–370.

Ferziger, J.H., Perić, M., 2008. Numerische Strömungsmechanik. Springer.

Hirano, K., Fabbro, R., Muller, M., 2011. Experimental determination of temperature threshold for melt surface deformation during laser interaction on iron at atmospheric pressure. J. Phys. D: Appl. Phys. 44, 435402.

Katayama, S., Kawahito, Y., Mizutani, M., 2010. Elucidation of laser welding phenomena and factors affecting weld penetration and welding defects, in: Schmidt, M., Vollertsen, F., Geiger, M. (Eds.), Physics Procedia, Volume 5, Elsevier. pp. 9–17.

Ki, H., Mohanty, P., Mazumder, J., 2001. Modelling of high-density laser-material interaction using fast level set method. Journal of Physics D: Applied Physics 34, 364.

Knight, C.J., 1972. Theoretical modeling of rapid surface vaporization with back pressure. AIAA Journal 17(5), 519–523.

Koch, H., Kägeler, C., Otto, A., Schmidt, M., 2011. Analysis of welding zinc coated steel sheets in zero gap configuration by 3d simulations and high speed imaging. Physics Procedia 12, 428–436.

Locke, E., Hoag, E., Hella, R., 1972. Deep penetration welding with high power co_2 lasers. Welding Journal 51(5), 245s–249s.

Miyamoto, I., Maruo, H., 1996. Evaporation characteristics in laser welding - fundamental study on theoretical modelling of laser welding. Welding International 10, No. 6, 448–453.

Mundra, K., Debroy, T., 1993. Toward understanding alloying element vaporization during laser beam welding of stainless steel. Welding journal 72(1), 1–s–9–s.

Otto, A., Schmidt, M., 2010. Towards a universal numerical simulation model for laser material processing. Physics Procedia 5, 35–46.

Seidgazov, R., 2009. Thermocapillary mechanism of melt displacement during keyhole formation by the laser beam. Journal of Physics D: Applied Physics 42, 175501–175508.

Semak, V., Matsunawa, A., 1997. The role of recoil pressure in energy balance during laser materials processing. J. Phys. D: Appl. Phys. 30, 2541–2552.

Serra, J., Vincent, L., 1992. An overview of morphological filtering. Circuits Systems and Signal Processing 11, 47–108. doi:10.1007/BF01189221.

Shcheglov, P., Gumenyuk, A., Gornushkin, I., Rethmeier, M., 2011. Experimental investigation of the laser-plume interaction during high power fiber laser welding, in: 30th international congress on applications of lasers & electro-optics, LIA. pp. 637–645.

Sibillano, T., Rizzi, D., Ancona, A., Saludes-Rodil, S., Rodriguez Nieto, J., Chmelickova, H., Sebestova, H., 2012. Spectroscopic monitoring of penetration depth in co_2 nd:yag and fiber laser welding processes. Journal of Materials Processing Technology 212, 910–916.

Sokolowinski, W., 1991. (in German) Diagnostik des laserinduzierten Plasmas beim Schweissen mit CO_2 Lasern. Verlag der Augustinus Buchhandlung, Aachen. chapter 3.4.1.

Tenner, F., Brock, C., Klämpfl, F., Schmidt, M., 2013. Isochronous high-speed video analysis of plasma plume, melt pool and keyhole behavior during laser metal welding, in: Proceedings of the 6th International Congress on Laser Advanced Materials Processing (LAMP2013), p. A050.

Versteeg, H.K., Malalasekera, W., 2007. An introduction to computational fluid dynamics: the finite volume method. Pearson Education.

Zhang, L., Zhang, J., Zhang, G., Bo, W., Gong, S., 2011. An investigation on the effects of side assisting gas flow and metallic vapour jet on the stability of keyhole and molten pool during laser full-penetration welding. J. Phys. D: Appl. Phys. 44, 135201.